

Observation of $\Lambda_c^+ \rightarrow \Lambda^0 K^+$, $\Lambda_c^+ \rightarrow \Sigma^0 K^+$ and
 $\Lambda_c^+ \rightarrow \Sigma^+ K^+ \pi^-$ decays

The Belle Collaboration

Abstract

We present measurements of the Cabibbo-suppressed decays $\Lambda_c^+ \rightarrow \Lambda^0 K^+$ and $\Lambda_c^+ \rightarrow \Sigma^0 K^+$ (both first observations), $\Lambda_c^+ \rightarrow \Sigma^+ K^+ \pi^-$ (seen with large statistics for the first time), $\Lambda_c^+ \rightarrow p K^+ K^-$ and $\Lambda_c^+ \rightarrow p \phi$ (measured with improved accuracy). Improved branching ratio measurements for the decays $\Lambda_c^+ \rightarrow \Sigma^+ K^+ K^-$ and $\Lambda_c^+ \rightarrow \Sigma^+ \phi$, which are attributed to W-exchange diagrams, are shown. We also present the first evidence for $\Lambda_c^+ \rightarrow \Xi(1690) K^+$ and set an upper limit on non-resonant $\Lambda_c^+ \rightarrow \Sigma^+ K^+ K^-$ decay. This analysis was performed using 23.6 fb^{-1} of data collected by the Belle detector at the e^+e^- asymmetric collider KEKB.

K. Abe⁹, K. Abe³⁷, R. Abe²⁷, I. Adachi⁹, Byoung Sup Ahn¹⁵, H. Aihara³⁹, M. Akatsu²⁰,
 K. Asai²¹, M. Asai¹⁰, Y. Asano⁴⁴, T. Aso⁴³, V. Aulchenko², T. Aushev¹³, A. M. Bakich³⁵,
 E. Banas²⁵, S. Behari⁹, P. K. Behera⁴⁵, D. Beilne², A. Bondar², A. Bozek²⁵,
 T. E. Browder⁸, B. C. K. Casey⁸, P. Chang²⁴, Y. Chao²⁴, K.-F. Chen²⁴, B. G. Cheon³⁴,
 R. Chistov¹³, S.-K. Choi⁷, Y. Choi³⁴, L. Y. Dong¹², J. Dragic¹⁸, A. Drutskoy¹³,
 S. Eidelman², V. Eiges¹³, Y. Enari²⁰, C. W. Everton¹⁸, F. Fang⁸, H. Fujii⁹, C. Fukunaga⁴¹,
 M. Fukushima¹¹, A. Garmash^{2,9}, A. Gordon¹⁸, K. Gotow⁴⁶, H. Guler⁸, R. Guo²², J. Haba⁹,
 H. Hamasaki⁹, K. Hanagaki³¹, F. Handa³⁸, K. Hara²⁹, T. Hara²⁹, N. C. Hastings¹⁸,
 H. Hayashii²¹, M. Hazumi²⁹, E. M. Heenan¹⁸, Y. Higasino²⁰, I. Higuchi³⁸, T. Higuchi³⁹,
 T. Hirai⁴⁰, H. Hirano⁴², T. Hojo²⁹, T. Hokuue²⁰, Y. Hoshi³⁷, K. Hoshina⁴², S. R. Hou²⁴,
 W.-S. Hou²⁴, S.-C. Hsu²⁴, H.-C. Huang²⁴, Y. Igarashi⁹, T. Iijima⁹, H. Ikeda⁹, K. Ikeda²¹,
 K. Inami²⁰, A. Ishikawa²⁰, H. Ishino⁴⁰, R. Itoh⁹, G. Iwai²⁷, H. Iwasaki⁹, Y. Iwasaki⁹,
 D. J. Jackson²⁹, P. Jalocha²⁵, H. K. Jang³³, M. Jones⁸, R. Kagan¹³, H. Kakuno⁴⁰,
 J. Kaneko⁴⁰, J. H. Kang⁴⁸, J. S. Kang¹⁵, P. Kapusta²⁵, N. Katayama⁹, H. Kawai³,
 H. Kawai³⁹, Y. Kawakami²⁰, N. Kawamura¹, T. Kawasaki²⁷, H. Kichimi⁹, D. W. Kim³⁴,
 Heejong Kim⁴⁸, H. J. Kim⁴⁸, Hyunwoo Kim¹⁵, S. K. Kim³³, T. H. Kim⁴⁸, K. Kinoshita⁵,
 S. Kobayashi³², S. Koishi⁴⁰, H. Konishi⁴², K. Korotushenko³¹, P. Krokovny², R. Kulasiri⁵,
 S. Kumar³⁰, T. Kuniya³², E. Kurihara³, A. Kuzmin², Y.-J. Kwon⁴⁸, J. S. Lange⁶,
 S. H. Lee³³, C. Leonidopoulos³¹, Y.-S. Lin²⁴, D. Liventsev¹³, R.-S. Lu²⁴, D. Marlow³¹,
 T. Matsubara³⁹, S. Matsui²⁰, S. Matsumoto⁴, T. Matsumoto²⁰, Y. Mikami³⁸, K. Misono²⁰,
 K. Miyabayashi²¹, H. Miyake²⁹, H. Miyata²⁷, L. C. Moffitt¹⁸, G. R. Moloney¹⁸,
 G. F. Moorhead¹⁸, N. Morgan⁴⁶, S. Mori⁴⁴, T. Mori⁴, A. Murakami³², T. Nagamine³⁸,
 Y. Nagasaka¹⁰, Y. Nagashima²⁹, T. Nakadaira³⁹, T. Nakamura⁴⁰, E. Nakano²⁸, M. Nakao⁹,
 H. Nakazawa⁴, J. W. Nam³⁴, Z. Natkaniec²⁵, K. Neichi³⁷, S. Nishida¹⁶, O. Nitoh⁴²,
 S. Noguchi²¹, T. Nozaki⁹, S. Ogawa³⁶, T. Ohshima²⁰, Y. Ohshima⁴⁰, T. Okabe²⁰,
 T. Okazaki²¹, S. Okuno¹⁴, S. L. Olsen⁸, H. Ozaki⁹, P. Pakhlov¹³, H. Palka²⁵, C. S. Park³³,
 C. W. Park¹⁵, H. Park¹⁷, L. S. Peak³⁵, M. Peters⁸, L. E. Piilonen⁴⁶, E. Prebys³¹,
 J. L. Rodriguez⁸, N. Root², M. Rozanska²⁵, K. Rybicki²⁵, J. Ryuko²⁹, H. Sagawa⁹,
 Y. Sakai⁹, H. Sakamoto¹⁶, M. Satapathy⁴⁵, A. Satpathy^{9,5}, S. Schrenk⁵, S. Semenov¹³,
 K. Senyo²⁰, Y. Settai⁴, M. E. Sevier¹⁸, H. Shibuya³⁶, B. Shwartz², A. Sidorov², S. Stanic⁴⁴,
 A. Sugi²⁰, A. Sugiyama²⁰, K. Sumisawa⁹, T. Sumiyoshi⁹, J.-I. Suzuki⁹, K. Suzuki³,
 S. Suzuki⁴⁷, S. Y. Suzuki⁹, S. K. Swain⁸, H. Tajima³⁹, T. Takahashi²⁸, F. Takasaki⁹,
 M. Takita²⁹, K. Tamai⁹, N. Tamura²⁷, J. Tanaka³⁹, M. Tanaka⁹, Y. Tanaka¹⁹,
 G. N. Taylor¹⁸, Y. Teramoto²⁸, M. Tomoto⁹, T. Tomura³⁹, S. N. Tovey¹⁸, K. Trabelsi⁸,
 T. Tsuboyama⁹, T. Tsukamoto⁹, S. Uehara⁹, K. Ueno²⁴, Y. Unno³, S. Uno⁹, Y. Ushiroda⁹,
 S. E. Vahsen³¹, K. E. Varvell³⁵, C. C. Wang²⁴, C. H. Wang²³, J. G. Wang⁴⁶, M.-Z. Wang²⁴,
 Y. Watanabe⁴⁰, E. Won³³, B. D. Yabsley⁹, Y. Yamada⁹, M. Yamaga³⁸, A. Yamaguchi³⁸,
 H. Yamamoto⁸, T. Yamanaka²⁹, Y. Yamashita²⁶, M. Yamauchi⁹, S. Yanaka⁴⁰,
 M. Yokoyama³⁹, K. Yoshida²⁰, Y. Yusa³⁸, H. Yuta¹, C. C. Zhang¹², J. Zhang⁴⁴,
 H. W. Zhao⁹, Y. Zheng⁸, V. Zhilich², and D. Žontar⁴⁴

¹Aomori University, Aomori

²Budker Institute of Nuclear Physics, Novosibirsk

³Chiba University, Chiba

⁴Chuo University, Tokyo

⁵University of Cincinnati, Cincinnati OH

- ⁶University of Frankfurt, Frankfurt
- ⁷Gyeongsang National University, Chinju
- ⁸University of Hawaii, Honolulu HI
- ⁹High Energy Accelerator Research Organization (KEK), Tsukuba
- ¹⁰Hiroshima Institute of Technology, Hiroshima
- ¹¹Institute for Cosmic Ray Research, University of Tokyo, Tokyo
- ¹²Institute of High Energy Physics, Chinese Academy of Sciences, Beijing
- ¹³Institute for Theoretical and Experimental Physics, Moscow
- ¹⁴Kanagawa University, Yokohama
- ¹⁵Korea University, Seoul
- ¹⁶Kyoto University, Kyoto
- ¹⁷Kyungpook National University, Taegu
- ¹⁸University of Melbourne, Victoria
- ¹⁹Nagasaki Institute of Applied Science, Nagasaki
- ²⁰Nagoya University, Nagoya
- ²¹Nara Women's University, Nara
- ²²National Kaohsiung Normal University, Kaohsiung
- ²³National Lien-Ho Institute of Technology, Miao Li
- ²⁴National Taiwan University, Taipei
- ²⁵H. Niewodniczanski Institute of Nuclear Physics, Krakow
- ²⁶Nihon Dental College, Niigata
- ²⁷Niigata University, Niigata
- ²⁸Osaka City University, Osaka
- ²⁹Osaka University, Osaka
- ³⁰Panjab University, Chandigarh
- ³¹Princeton University, Princeton NJ
- ³²Saga University, Saga
- ³³Seoul National University, Seoul
- ³⁴Sungkyunkwan University, Suwon
- ³⁵University of Sydney, Sydney NSW
- ³⁶Toho University, Funabashi
- ³⁷Tohoku Gakuin University, Tagajo
- ³⁸Tohoku University, Sendai
- ³⁹University of Tokyo, Tokyo
- ⁴⁰Tokyo Institute of Technology, Tokyo
- ⁴¹Tokyo Metropolitan University, Tokyo
- ⁴²Tokyo University of Agriculture and Technology, Tokyo
- ⁴³Toyama National College of Maritime Technology, Toyama
- ⁴⁴University of Tsukuba, Tsukuba
- ⁴⁵Utkal University, Bhubaneswer
- ⁴⁶Virginia Polytechnic Institute and State University, Blacksburg VA
- ⁴⁷Yokkaichi University, Yokkaichi
- ⁴⁸Yonsei University, Seoul

I. INTRODUCTION

Decays of charmed baryons, unlike charmed mesons, are not colour or helicity suppressed, allowing us to investigate the contribution of W-exchange diagrams. There are also possible interference effects due to the presence of identical quarks. This makes the study of these decays a useful tool to test theoretical models that predict exclusive decay rates [1].

During the past several years there has been significant progress in the experimental study of hadronic decays of charmed baryons. New results on masses, widths, lifetimes and asymmetry decay parameters have been published by various experiments [2]. However the accuracy of branching ratio measurements does not exceed 30% for many Cabibbo-favoured modes: for Cabibbo-suppressed and W-exchange dominated decays, the experimental accuracy is even worse. As a result, we are not yet able to conclusively distinguish between the decay rate predictions made by different theoretical models.

In this paper we present a study of Λ_c^+ baryons produced in the $e^+e^- \rightarrow q\bar{q}$ continuum at Belle, relying on the excellent particle identification system of the detector to measure decays with kaons in the final state. We report the first observation of the Cabibbo-suppressed decays $\Lambda_c^+ \rightarrow \Lambda^0 K^+$ and $\Lambda_c^+ \rightarrow \Sigma^0 K^+$, and the first observation of $\Lambda_c^+ \rightarrow \Sigma^+ K^+ \pi^-$ with large statistics. (Here and throughout this paper, the inclusion of charge-conjugate states is implied.) We present improved measurements of the Cabibbo-suppressed decays $\Lambda_c^+ \rightarrow p K^+ K^-$ and $\Lambda_c^+ \rightarrow p \phi$, and the W-exchange decays $\Lambda_c^+ \rightarrow \Sigma^+ K^+ K^-$ and $\Lambda_c^+ \rightarrow \Sigma^+ \phi$; we also report the first evidence for $\Lambda_c^+ \rightarrow \Xi(1690) K^+$, and set an upper limit on non-resonant $\Lambda_c^+ \rightarrow \Sigma^+ K^+ K^-$ decay. All branching ratio measurements and limits are preliminary.

II. DATA AND SELECTION CRITERIA

The data used for this analysis were taken on the $\Upsilon(4S)$ resonance and in the nearby continuum using the Belle detector at the e^+e^- asymmetric collider KEKB. The integrated luminosity of the data sample is equal to 23.6 fb^{-1} .

Belle is a general purpose detector based on a 1.5 T superconducting solenoid; a detailed description can be found elsewhere [3]. Tracking is performed by a silicon vertex detector (SVD) composed of three concentric layers of double sided silicon strip detectors, and a 50 layer drift chamber. Particle identification for charged hadrons, important for the measurement of final states with kaons and/or protons, is based on the combination of energy loss measurements (dE/dx) in the drift chamber, time of flight measurements and aerogel Čerenkov counter information. For each charged track, measurements from these three sub-detectors are combined to form K/π and p/K likelihood ratios in the range from 0 to 1,

$$P(K/\pi) = \mathcal{L}(K)/(\mathcal{L}(K) + \mathcal{L}(\pi)), \quad P(p/K) = \mathcal{L}(p)/(\mathcal{L}(p) + \mathcal{L}(K)),$$

where $\mathcal{L}(p)$, $\mathcal{L}(K)$ and $\mathcal{L}(\pi)$ are the likelihood values assigned to each identification hypothesis for a given track.

For the analyses presented here, we require $P(K/\pi) < 0.9$ for pions, $P(K/\pi) > 0.6$ for kaons, and $P(p/K) > 0.9$ for protons unless otherwise stated. Candidate π^0 's are reconstructed from pairs of photons detected in the CsI calorimeter, with a minimum energy of 50 MeV per photon. Other particles are identified as follows:

- Λ^0 are reconstructed in the decay mode $\Lambda^0 \rightarrow p\pi^-$, fitting the p and π tracks to a common vertex and requiring an invariant mass in a $\pm 3\text{MeV}/c^2$ ($\approx 3\sigma$) interval around the nominal value. The likelihood ratio cut on the proton is relaxed to $P(p/K) > 0.4$. We then make the following cuts on the Λ^0 decay vertex:

- the difference Z_{dist} in z -coordinate between the proton and pion at the decay vertex must satisfy $Z_{\text{dist}} < 1$ cm;
- the distance between the vertex position and interaction point (IP) in the $r - \phi$ plane must be > 1 mm;
- the angle α , between the Λ^0 momentum vector and the vector pointing from the IP to the decay vertex, must satisfy $\cos \alpha > 0.995$.

Finally, to reduce the combinatorial background, we require the Λ^0 momentum to be greater than $1.5\text{ GeV}/c$.

- Σ^+ are reconstructed in the decay mode $\Sigma^+ \rightarrow p\pi^0$, requiring an invariant mass within $\pm 10\text{ MeV}/c^2$ ($\approx 2.0\sigma$) of the nominal value. Since the Σ^+ mass resolution is dominated by the uncertainty in the π^0 momentum, rather than the choice of Σ^+ decay vertex, we use the IP to estimate the vertex for the π^0 fit; this approximation has been checked in the Monte Carlo. The displaced Σ^+ vertex is taken into account using the impact parameter of the decay proton in the $r - \phi$ plane with respect to the IP, $d_{r\phi}$. We require the proton to have at least one hit in the SVD, to improve the impact parameter resolution, and then make a cut $d_{r\phi} > 500\text{ }\mu\text{m}$.
- $\Sigma^0 \rightarrow \Lambda^0\gamma$ decays are formed using identified Λ^0 and photons with calorimeter cluster energies $E_\gamma > 0.1\text{ GeV}$; we accept candidates with invariant masses within $\pm 6\text{ MeV}/c^2$ ($\approx 1.5\sigma$) of the nominal value. To suppress the background from slow photons, the cosine of the angle between the γ in the Σ^0 rest frame and the Σ^0 boost direction is required to be greater than -0.8 .

To suppress combinatorial and $B\bar{B}$ backgrounds, we require Λ_c^+ candidates to have scaled momentum $x_p = p^*(\Lambda_c^+)/\sqrt{E_{CMS}^2/4 - M^2} > 0.5$, where $p^*(\Lambda_c^+)$ and E_{CMS} are the candidate momentum and total e^+e^- beam energy in the center of mass frame, respectively, and M the reconstructed mass of the Λ_c^+ . In modes where there are two or more charged tracks at the Λ_c^+ vertex, we perform a vertex fit and require $\chi^2/\text{n.d.f.} < 9$.

III. FIRST OBSERVATION OF THE DECAYS $\Lambda_c^+ \rightarrow \Lambda^0 K^+$ AND $\Lambda_c^+ \rightarrow \Sigma^0 K^+$

The Cabibbo-suppressed decay $\Lambda_c^+ \rightarrow \Lambda^0 K^+$ has not previously been observed. Reconstructing $\Lambda^0 K^+$ combinations as described in section II, we see a clear signal at the Λ_c^+ mass, as shown in Fig. 1(a).

To study backgrounds due to Cabibbo-allowed decays, we reconstruct a second sample with a tight pion identification cut $P(K/\pi) < 0.1$ applied to the “kaon”, Fig. 1(b); the kaon mass hypothesis is still used in this case. We see a broad structure centered around $2400\text{ MeV}/c^2$: using the MC simulation we find that this is produced by Cabibbo-allowed $\Lambda_c^+ \rightarrow \Lambda^0 \pi^+$ and $\Lambda_c^+ \rightarrow \Sigma^0 \pi^+$ decays. The background due to $\Lambda_c^+ \rightarrow \Sigma^0 \pi^+$ is dangerous,

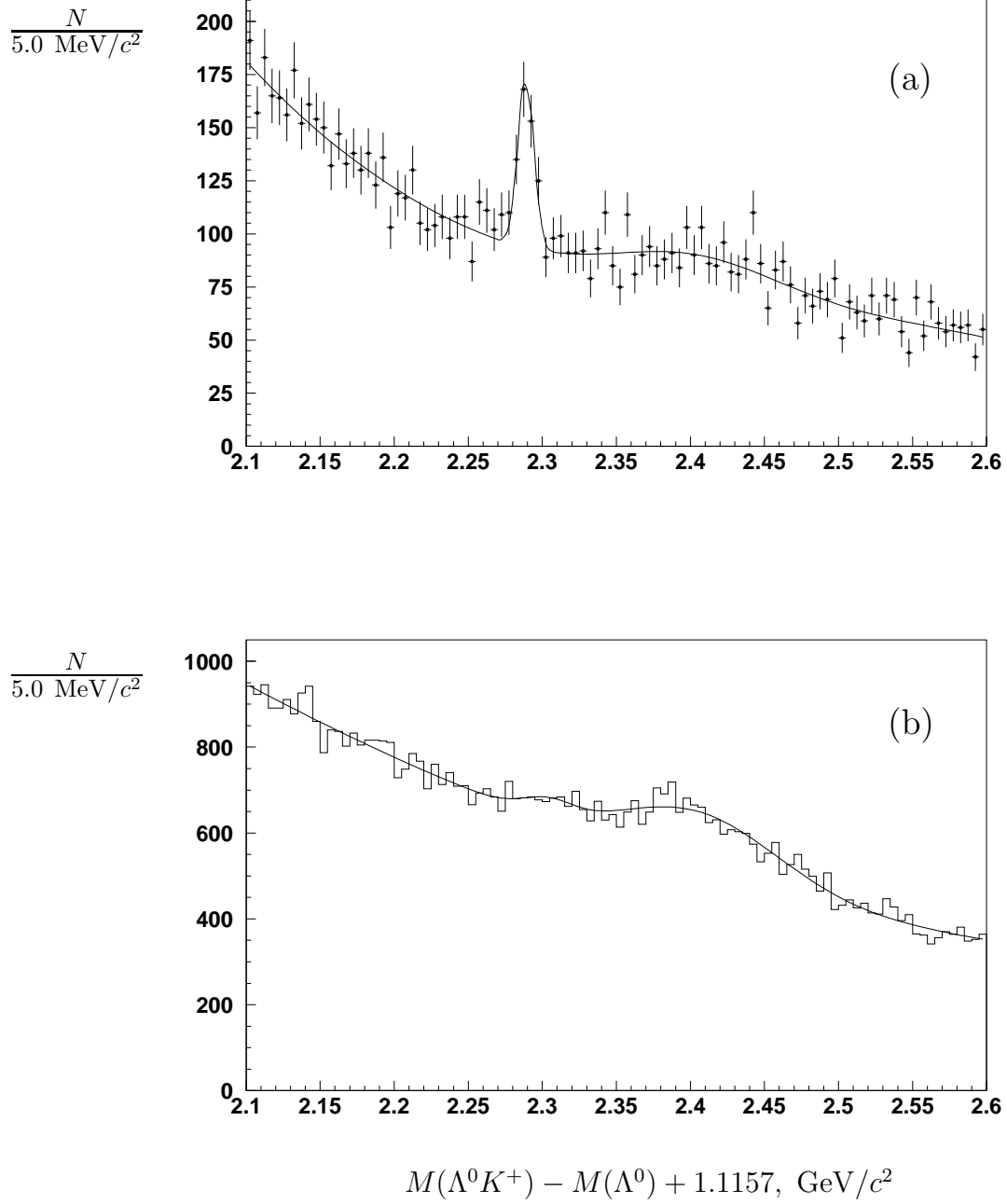


FIG. 1. $\Lambda_c^+ \rightarrow \Lambda^0 K^+$: invariant mass spectra of the selected $\Lambda^0 K^+$ combinations. Plot (a) is made with the requirement $P(K/\pi) > 0.6$ on the kaon candidate. Plot (b) is made with the requirement $P(K/\pi) < 0.1$ to get the form of the contribution from misidentified pions. The other selection requirements and the fitting procedure are described in the text. The structure near $2.4 \text{ GeV}/c^2$ is due to misidentified $\Lambda_c^+ \rightarrow \Lambda^0 \pi^+$ and $\Lambda_c^+ \rightarrow \Sigma^0 \pi^+$ decays.

since the mass shifts due to the undetected γ (from $\Sigma^0 \rightarrow \Lambda^0 \gamma$) and $\pi \rightarrow K$ misidentification partially cancel, leaving a peak close to the Λ_c^+ mass. Feed-downs from other Cabibbo-allowed Λ_c decays, $\Lambda_c^+ \rightarrow \Lambda^0 \pi^+ \pi^0$, $\Lambda_c^+ \rightarrow \Lambda^0 \pi^+ \pi^+ \pi^-$ and $\Lambda_c^+ \rightarrow \Sigma^0 \pi^+ \pi^0$, produce broad reflections due to the missing particle(s), and no prominent structures are seen. We therefore fit the distribution using two gaussians with floating central values and widths (to model the $\Lambda_c^+ \rightarrow \Lambda^0 \pi^+$ and $\Lambda_c^+ \rightarrow \Sigma^0 \pi^+$ contributions), and a second order polynomial (to model the wide reflections and the remaining background); the result of the fit is superimposed on Fig. 1(b). All parameters except for the overall normalization are then fixed, and we use this function to model the $\Lambda^0 \pi^+$ background in the main sample (Fig. 1(a)).

The remaining combinatorial background in Fig. 1(a) is represented using a second order polynomial, and the $\Lambda_c^+ \rightarrow \Lambda^0 K^+$ signal is described by a gaussian with width $\sigma = 5.4 \text{ MeV}/c^2$ (fixed from MC); the result of the fit is shown by the superimposed curve. We find a yield of 214 ± 30 $\Lambda_c^+ \rightarrow \Lambda^0 K^+$ decays, the first observation of this decay mode.

For normalization, we use the decay $\Lambda_c^+ \rightarrow \Lambda^0 \pi^+$: the mass distribution of the candidates is shown in Fig. 2. A fit with a gaussian with a floating width for the signal and a second order polynomial for the background (restricted to the region above the $\Lambda_c^+ \rightarrow \Sigma^0 \pi^+$ reflection) yields 3270 ± 95 events; the fitted signal width $\sigma = 6.6 \pm 0.2 \text{ MeV}/c^2$ is consistent with the MC prediction of $6.8 \text{ MeV}/c^2$. The relative reconstruction efficiency is found to be $\epsilon(\Lambda_c^+ \rightarrow \Lambda^0 K^+)/\epsilon(\Lambda_c^+ \rightarrow \Lambda^0 \pi^+) = 0.18/0.23 = 0.77$ in the Monte Carlo: using this value, we extract the branching ratio

$$\mathcal{B}(\Lambda_c^+ \rightarrow \Lambda^0 K^+)/\mathcal{B}(\Lambda_c^+ \rightarrow \Lambda^0 \pi^+) = 0.085 \pm 0.012 \pm 0.015.$$

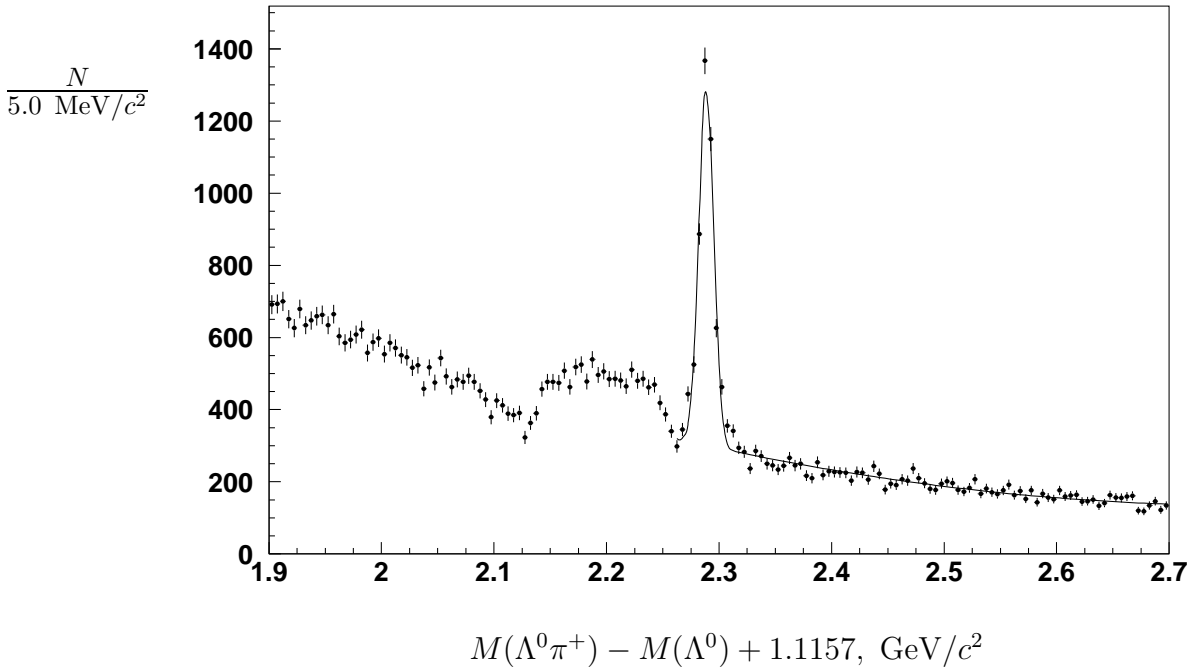


FIG. 2. The invariant mass spectrum for the normalization mode $\Lambda_c^+ \rightarrow \Lambda^0 \pi^+$. The selection requirements and fit are described in the text. The broad feature below the Λ_c^+ mass is due to $\Lambda_c^+ \rightarrow \Sigma^0 \pi^+$ decays.

The first error is statistical, and the second is systematic, combining the effects of uncertainties in K/π identification efficiencies and the result of varying the ranges and parameters of the fits.

The Cabibbo-suppressed decay $\Lambda_c^+ \rightarrow \Sigma^0 K^+$ is reconstructed in a similar way, with the scaled momentum cut tightened to $x_p > 0.6$ to suppress the large background due to soft photons. The invariant mass distribution of the selected $\Sigma^0 K^+$ candidates is shown in Fig. 3: a peak is seen at the Λ_c^+ mass, and a reflection due to misidentified two-body Cabibbo-allowed Λ_c^+ decays is seen at higher masses. The superimposed curve shows the result of a fit constructed using the method described for $\Lambda^0 K^+$, with the exception that the width of the signal gaussian is fixed from the Monte Carlo to $\sigma = 5.0 \text{ MeV}/c^2$ in this case. We find $70 \pm 17 \Lambda_c^+ \rightarrow \Sigma^0 K^+$ events, the first observation of this decay mode.

For normalization, we use the decay $\Lambda_c^+ \rightarrow \Sigma^0 \pi^+$, shown in Fig. 4. We fit the distribution with a gaussian for the signal, a second gaussian to describe the broad bump due to $\Lambda_c^+ \rightarrow \Lambda^0 \pi^+$ (with the addition of a random γ), and a second order polynomial for the remaining background. The mean of the signal gaussian is fixed at the Λ_c^+ mass, and all other parameters are allowed to float: the fitted width of the signal $\sigma = 5.7 \pm 0.2 \text{ MeV}/c^2$ is consistent with the MC prediction $\sigma = 6.1 \text{ MeV}/c^2$. The fit gives $1132 \pm 39 \Lambda_c^+ \rightarrow \Sigma^0 \pi^+$ decays. The relative reconstruction efficiency is found to be $\epsilon(\Lambda_c^+ \rightarrow \Sigma^0 K^+)/\epsilon(\Lambda_c^+ \rightarrow \Sigma^0 \pi^+) = 0.096/0.114 = 0.84$ in the Monte Carlo: we then extract the branching ratio

$$\mathcal{B}(\Lambda_c^+ \rightarrow \Sigma^0 K^+)/\mathcal{B}(\Lambda_c^+ \rightarrow \Sigma^0 \pi^+) = 0.073 \pm 0.018 \pm 0.016.$$

The first error is statistical, and the second is systematic, combining uncertainties from particle identification efficiencies and the fitting procedure.

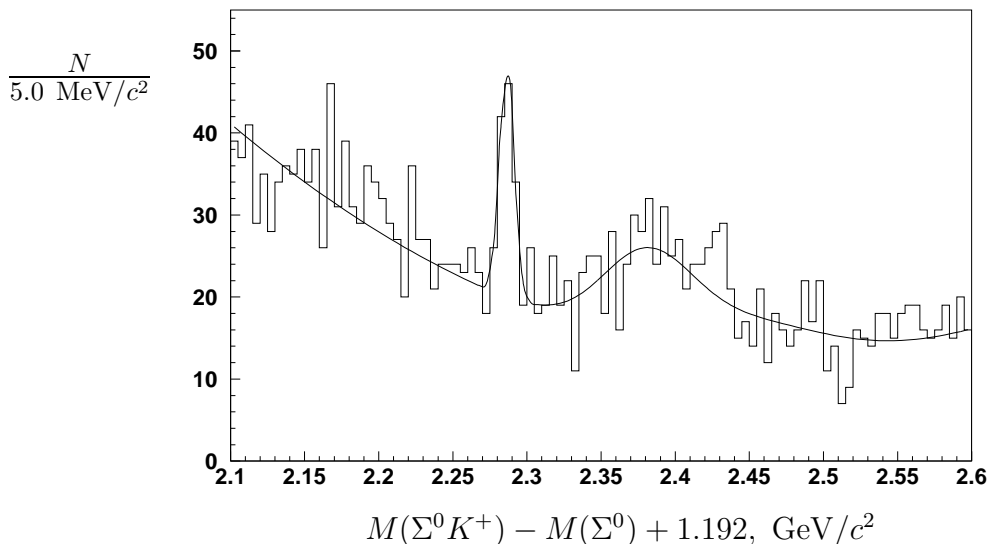


FIG. 3. $\Lambda_c^+ \rightarrow \Sigma^0 K^+$: invariant mass spectrum of the selected $\Sigma^0 K^+$ combinations. The selection requirements and fit are described in the text.

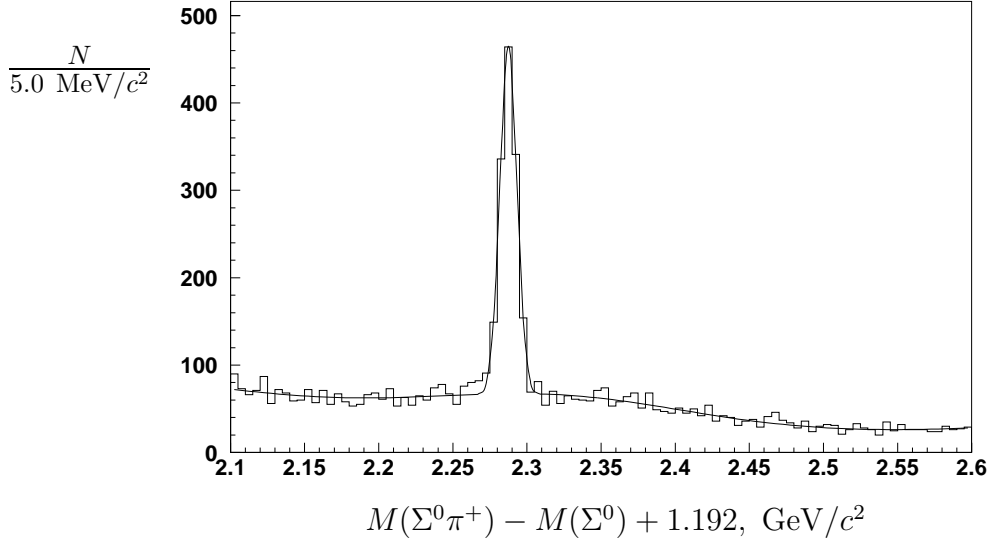


FIG. 4. The invariant mass spectrum for the normalization mode $\Lambda_c^+ \rightarrow \Sigma^0 \pi^+$. The selection requirements and fit are described in the text. The broad enhancement around the Λ_c^+ mass region is due to $\Lambda_c^+ \rightarrow \Lambda^0 \pi^+$ decays.

IV. OBSERVATION OF THE $\Lambda_c^+ \rightarrow \Sigma^+ K^+ \pi^-$ DECAY

The first evidence for the Cabibbo-suppressed decay $\Lambda_c^+ \rightarrow \Sigma^+ K^+ \pi^-$ was published by the NA32 collaboration in 1992 [4]: they found 2 events in the signal region. Reconstructing $\Sigma^+ K^+ \pi^-$ combinations with the cuts of section II tightened to require $P(K/\pi) > 0.9$ for the kaon, and $x_p > 0.6$, we see a clear signal peak at the Λ_c^+ mass, as shown in Fig. 5. Tighter cuts are used to suppress the large combinatorial background. We also form $\Sigma^+ K^+ \pi^-$ combinations using “ Σ^+ ” candidates from mass sidebands ($> 2\sigma$ away from the nominal Σ^+ mass), shown with the shaded histogram: no enhancement is seen near the Λ_c^+ mass.

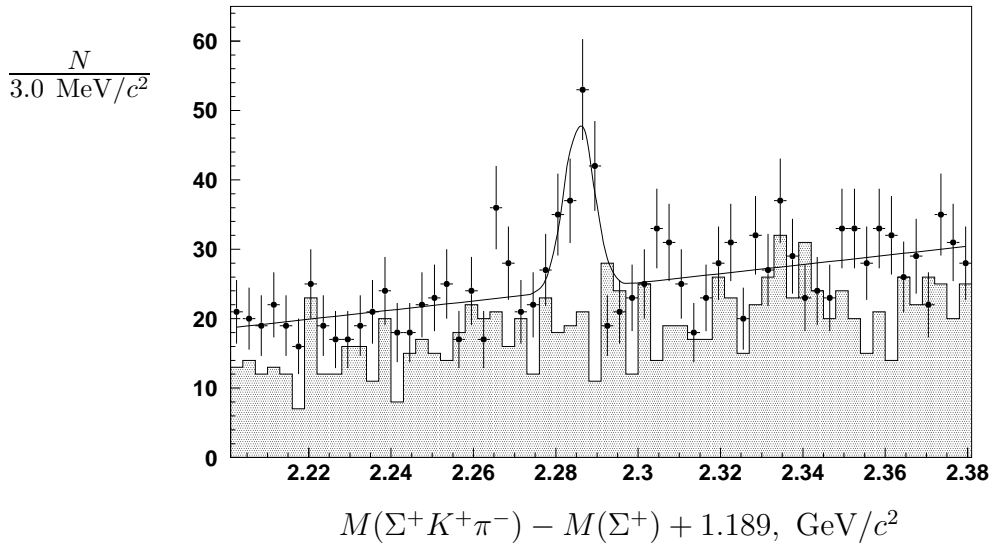


FIG. 5. $\Lambda_c^+ \rightarrow \Sigma^+ K^+ \pi^-$: invariant mass spectrum of the selected $\Sigma^+ K^+ \pi^-$ combinations. The shaded histogram shows the equivalent spectrum for the Σ^+ sidebands.

The mass distribution is fitted with a gaussian for the signal (with width fixed to $3.6 \text{ MeV}/c^2$ from the MC) and a first order polynomial for the background: we find 72 ± 16 $\Lambda_c^+ \rightarrow \Sigma^+ K^+ \pi^-$ events. For normalization we reconstructed $\Lambda_c^+ \rightarrow \Sigma^+ \pi^+ \pi^-$ decays with the same cuts, finding 1432 ± 78 events. The relative efficiency of the $\Lambda_c^+ \rightarrow \Sigma^+ K^+ \pi^-$ channel reconstruction with respect to $\Lambda_c^+ \rightarrow \Sigma^+ \pi^+ \pi^-$ was found to be $0.046/0.055 = 0.85$ in the Monte Carlo: using this value, we extract the branching ratio

$$\mathcal{B}(\Lambda_c^+ \rightarrow \Sigma^+ K^+ \pi^-)/\mathcal{B}(\Lambda_c^+ \rightarrow \Sigma^+ \pi^+ \pi^-) = 0.059 \pm 0.014 \pm 0.006;$$

the systematic error (quoted second) is dominated by the uncertainty in the relative K/π identification efficiency.

V. MEASUREMENT OF THE $\Lambda_c^+ \rightarrow \Sigma^+ K^+ K^-$ AND $\Lambda_c^+ \rightarrow \Sigma^+ \phi$ DECAYS

The decays $\Lambda_c^+ \rightarrow \Sigma^+ K^+ K^-$ and $\Lambda_c^+ \rightarrow \Sigma^+ \phi$ proceed dominantly via W-exchange diagrams, and were observed by CLEO in 1993 [5] with branching ratios $\mathcal{B}(\Lambda_c^+ \rightarrow \Sigma^+ K^+ K^-)/\mathcal{B}(\Lambda_c^+ \rightarrow p K^- \pi^+) = 0.070 \pm 0.012 \pm 0.011$ and $\mathcal{B}(\Lambda_c^+ \rightarrow \Sigma^+ \phi)/\mathcal{B}(\Lambda_c^+ \rightarrow p K^- \pi^+) = 0.069 \pm 0.023 \pm 0.016$. Here we measure these decay channels with improved accuracy and provide the first evidence for the $\Lambda_c^+ \rightarrow \Xi(1690)^0 K^+$ decay.

Fig. 6 shows the invariant mass spectrum for $\Lambda_c^+ \rightarrow \Sigma^+ K^+ K^-$ combinations selected according to section II, with the kaon cuts tightened to $P(K/\pi) > 0.9$, and the impact parameter cut for the proton from $\Sigma^+ \rightarrow p \pi^0$ relaxed to $d_{r\phi} > 200 \mu\text{m}$. A clear peak is seen at the Λ_c^+ mass, over a low background. We fit the distribution using a gaussian (with width fixed to $2.2 \text{ MeV}/c^2$ from the MC) plus a second order polynomial: the fit yields 161 ± 16 $\Lambda_c^+ \rightarrow \Sigma^+ K^+ K^-$ decays. For normalization we reconstructed the $\Lambda_c^+ \rightarrow \Sigma^+ \pi^+ \pi^-$ decay mode with equivalent cuts, shown in Fig. 7, and fitted the distribution in the same manner: we find 2759 ± 138 $\Lambda_c^+ \rightarrow \Sigma^+ \pi^+ \pi^-$ events. The relative efficiency of the $\Lambda_c^+ \rightarrow \Sigma^+ K^+ K^-$ decay reconstruction with respect to the $\Lambda_c^+ \rightarrow \Sigma^+ \pi^+ \pi^-$ decay was calculated by MC simulation and was found to be $0.052/0.067 = 0.78$. We thus extract a branching ratio

$$\mathcal{B}(\Lambda_c^+ \rightarrow \Sigma^+ K^+ K^-)/\mathcal{B}(\Lambda_c^+ \rightarrow \Sigma^+ \pi^+ \pi^-) = (7.5 \pm 0.8 \pm 1.5) \times 10^{-2},$$

where the second (systematic) error is dominated by the uncertainty in the relative K/π identification efficiency.

In order to obtain the $\Lambda_c^+ \rightarrow \Sigma^+ \phi$ signal, we take $\Sigma^+ K^+ K^-$ from a $\pm 5 \text{ MeV}/c^2$ window around the fitted Λ_c^+ mass ($2286 \text{ MeV}/c^2$), and plot the invariant mass of the $K^+ K^-$ combination, Fig. 8 (points with error bars); the equivalent distribution is also shown for $\Sigma^+ K^+ K^-$ in sidebands centred $10 \text{ MeV}/c^2$ below and above the fitted Λ_c^+ mass (shaded histogram). The distributions are fitted with a Breit-Wigner function (describing the ϕ signal) convoluted with a gaussian of a fixed width (representing the detector mass resolution) plus a 2nd order polynomial multiplied by a square root threshold factor. The intrinsic width of the ϕ Breit-Wigner function was fixed to its nominal value [2], and the width of the gaussian resolution was fixed to $1.0 \text{ MeV}/c^2$ based on the MC simulation. The fit yields 106 ± 12 events for the ϕ signal in the Λ_c^+ region and 15 ± 6 in the Λ_c^+ sidebands. To extract the $\Lambda_c^+ \rightarrow \Sigma^+ \phi$ contribution we subtract the ϕ yield in the sidebands from the yield in the Λ_c^+ signal region, correcting for the phase space factor obtained from the $\Sigma^+ K^+ K^-$ background

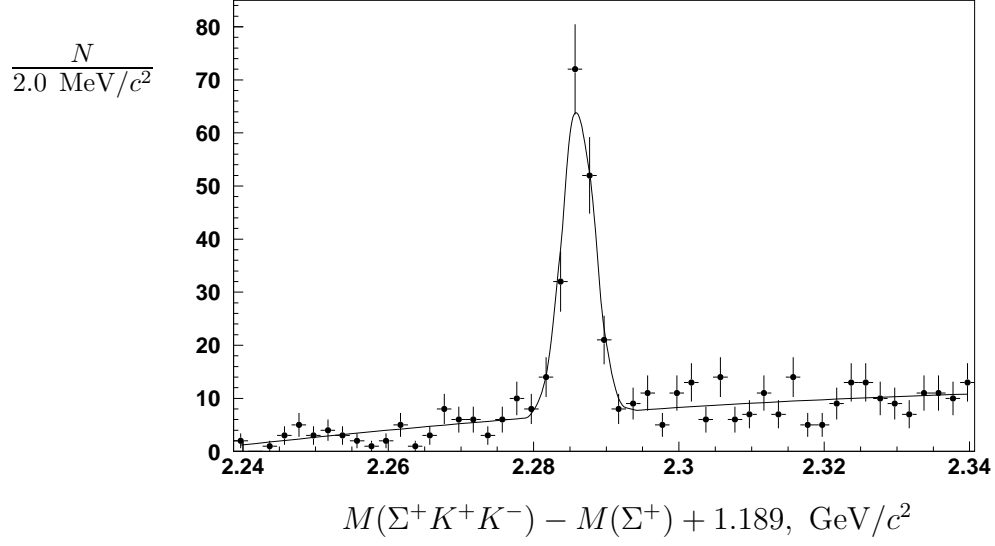


FIG. 6. $\Lambda_c^+ \rightarrow \Sigma^+ K^+ K^-$: invariant mass spectrum of the selected $\Sigma^+ K^+ K^-$ combinations.

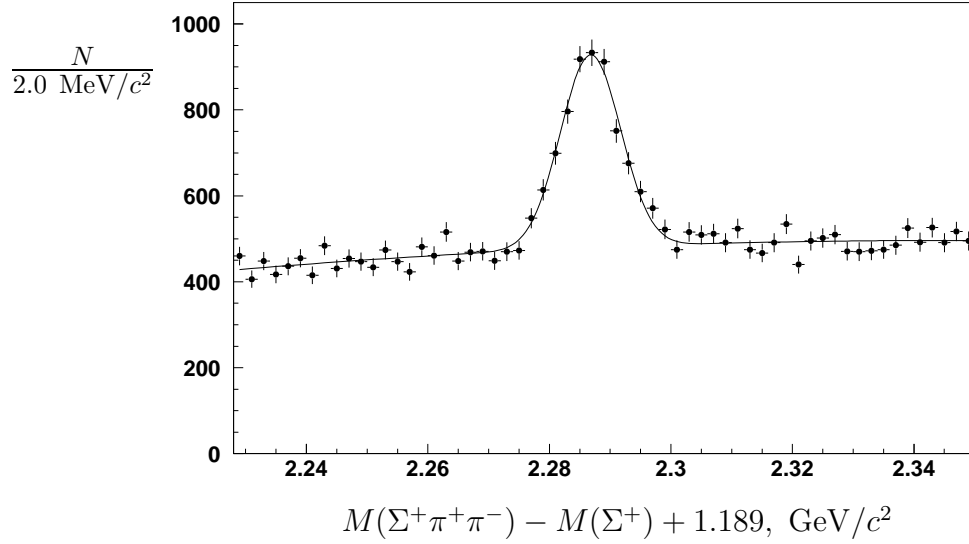


FIG. 7. The invariant mass spectrum for the normalization mode $\Lambda_c^+ \rightarrow \Sigma^+ \pi^+ \pi^-$, using equivalent cuts to the $\Lambda_c^+ \rightarrow \Sigma^+ K^+ K^-$ analysis.

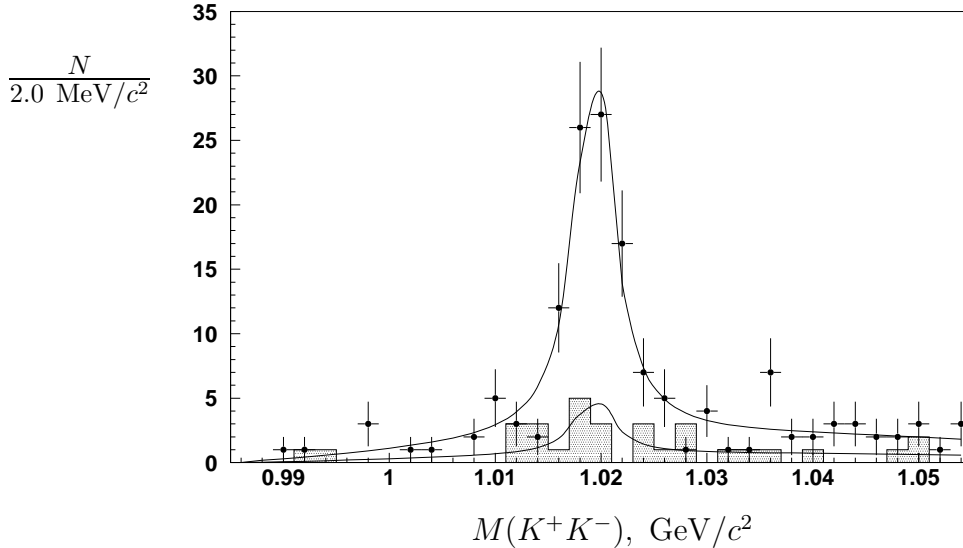


FIG. 8. Fitting for the $\Lambda_c^+ \rightarrow \Sigma^+ \phi$ component: the invariant mass spectra of $K^+ K^-$ combinations from the $\Lambda_c^+ \rightarrow \Sigma^+ K^+ K^-$ signal area (points with error bars) and Λ_c^+ sidebands (shaded histogram) are shown. The selection requirements and fit are described in the text.

fitting function. After making a further correction for the missing signal outside the Λ_c^+ mass interval, we obtain 93 ± 14 $\Lambda_c^+ \rightarrow \Sigma^+ \phi$ decays.

The relative efficiency of the $\Lambda_c^+ \rightarrow \Sigma^+ \phi$ reconstruction with respect to $\Lambda_c^+ \rightarrow \Sigma^+ \pi^+ \pi^-$ was calculated using the Monte Carlo and found to be $0.050/0.067 = 0.76$. Taking into account the ϕ branching fraction $\mathcal{B}(\phi \rightarrow K^+ K^-) = 49.2\%$ [2], we calculate a branching ratio

$$\mathcal{B}(\Lambda_c^+ \rightarrow \Sigma^+ \phi) / \mathcal{B}(\Lambda_c^+ \rightarrow \Sigma^+ \pi^+ \pi^-) = (9.1 \pm 1.4 \pm 1.8) \times 10^{-2}.$$

The systematic error of 1.8×10^{-2} is an estimate based on uncertainties in the relative K/π identification efficiency, and fit variations. In this case there is an additional source of systematic error due to the difference in kinematics between the signal and normalization modes: this has not yet been taken into account.

We also searched for the resonant structure in the $\Sigma^+ K^-$ system in $\Lambda_c^+ \rightarrow \Sigma^+ K^+ K^-$ decays. Fig. 9 shows the $\Sigma^+ K^-$ invariant mass spectra for $\Sigma^+ K^+ K^-$ combinations in a ± 5 MeV/ c^2 interval around the fitted Λ_c^+ mass (data points): we also required $|M(K^+ K^-) - m_\phi| > 10$ MeV/ c^2 to suppress $\phi \rightarrow K^+ K^-$. Also shown are $\Sigma^+ K^-$ from $\Sigma^+ K^+ K^-$ combinations selected inside ± 5 MeV/ c^2 sideband intervals 10 MeV/ c^2 below and above the fitted Λ_c^+ mass (shaded histogram). The $\Sigma^+ K^-$ mass distribution shows evidence for the $\Xi(1690)^0$ resonant state. In order to extract this resonant contribution the histograms were fitted with a Breit-Wigner function (describing the $\Xi(1690)^0$ signal) plus a 3rd order polynomial multiplied by a square root threshold factor. The fit yields 52.5 ± 15.0 events for the $\Xi(1690)^0$ signal in the Λ_c^+ region, with a fitted mass and width in good agreement with previous measurements of the $\Xi(1690)^0$ parameters [2]. To fit the sidebands, the function parameters were fixed to the central values obtained from the signal fit, and the normalization was floated: a yield of 7.2 ± 2.8 events was found.

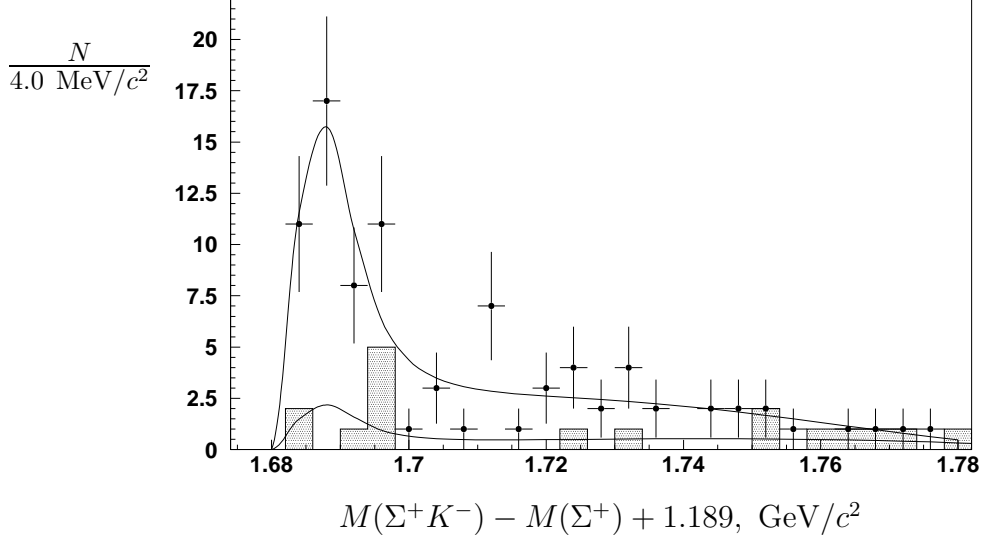


FIG. 9. Fitting for the $\Lambda_c^+ \rightarrow \Xi(1690)^0 K^+$ component: the invariant mass spectrum of $\Sigma^+ K^-$ combinations from the $\Lambda_c^+ \rightarrow \Sigma^+ K^+ K^-$ signal area (points with error bars) and Λ_c^+ sidebands (shaded histogram) are shown, with the $\phi \rightarrow K^+ K^-$ signal region excluded in both cases. The selection requirements and fit are described in the text.

The $\Lambda_c^+ \rightarrow \Xi(1690)^0 K^+$ contribution was obtained by subtracting the $\Xi(1690)^0$ yield in the sidebands from the yield in the Λ_c^+ signal region, correcting the sideband contribution using the phase space factor obtained from the $\Sigma^+ K^+ K^-$ background fitting function. After a further correction for the missing signal outside the Λ_c^+ mass interval, we obtained 45 ± 15 $\Lambda_c^+ \rightarrow \Xi(1690)^0 K^+$ decays. Assuming the relative efficiency for reconstruction of the $\Lambda_c^+ \rightarrow \Xi(1690)^0 K^+$ channel with respect to $\Lambda_c^+ \rightarrow \Sigma^+ \pi^+ \pi^-$ to be the same as for the inclusive $\Sigma^+ K^+ K^-$ mode, we find a combined branching ratio

$$\frac{\mathcal{B}(\Lambda_c^+ \rightarrow \Xi(1690)^0 K^+)}{\mathcal{B}(\Lambda_c^+ \rightarrow \Sigma^+ \pi^+ \pi^-)} \times \mathcal{B}(\Xi(1690)^0 \rightarrow \Sigma^+ K^-) = (2.1 \pm 0.7 \pm 0.4) \times 10^{-2};$$

where we have neglected possible effects due to interference with $\Lambda_c^+ \rightarrow \Sigma^+ \phi$, *etc.*

Finally, the non-resonant $\Lambda_c^+ \rightarrow \Sigma^+ K^+ K^-$ contribution is estimated by making invariant mass cuts $|M(K^+ K^-) - m_\phi| > 10 \text{ MeV}/c^2$ and $|M(\Sigma^+ K^-) - M_{\Xi(1690)}| > 20 \text{ MeV}/c^2$ to suppress the ϕ and $\Xi(1690)^0$ contributions (here, $M_{\Xi(1690)}$ is the fitted $\Xi(1690)^0$ mass): the resulting $\Sigma^+ K^+ K^-$ mass spectrum is shown in Fig. 10. A fit with a gaussian (with width fixed to $2.2 \text{ MeV}/c^2$ from the MC) plus a first order polynomial, shown on the figure, yields 23.8 ± 7.1 events. Integrating the ϕ Breit-Wigner function over the allowed $M(K^+ K^-)$ region, we found that 14% of the total $\Lambda_c^+ \rightarrow \Sigma^+ \phi$ signal contributes to this sample: 12.3 ± 2.5 events. The contribution of the $\Xi(1690)^0$ mass tails is estimated to be approximately 12% of the fitted $\Xi(1690)^0$ signal: 5.4 ± 1.8 events. Subtracting these contributions, 6.1 ± 7.7 non-resonant events remain. The phase space correction factor to account for the missing region around the ϕ and $\Xi(1690)^0$ masses is found to be 1.63 by MC simulation of the non-resonant $M(K^+ K^-)$ spectrum: applying this correction we obtain 9.9 ± 12.6 $\Lambda_c^+ \rightarrow \Sigma^+ K^+ K^-$ non-resonant decays. The relative efficiency for the reconstruction of the $\Lambda_c^+ \rightarrow \Sigma^+ K^+ K^-$ (non-resonant) channel with respect to the $\Lambda_c^+ \rightarrow \Sigma^+ \pi^+ \pi^-$ channel was taken to be the

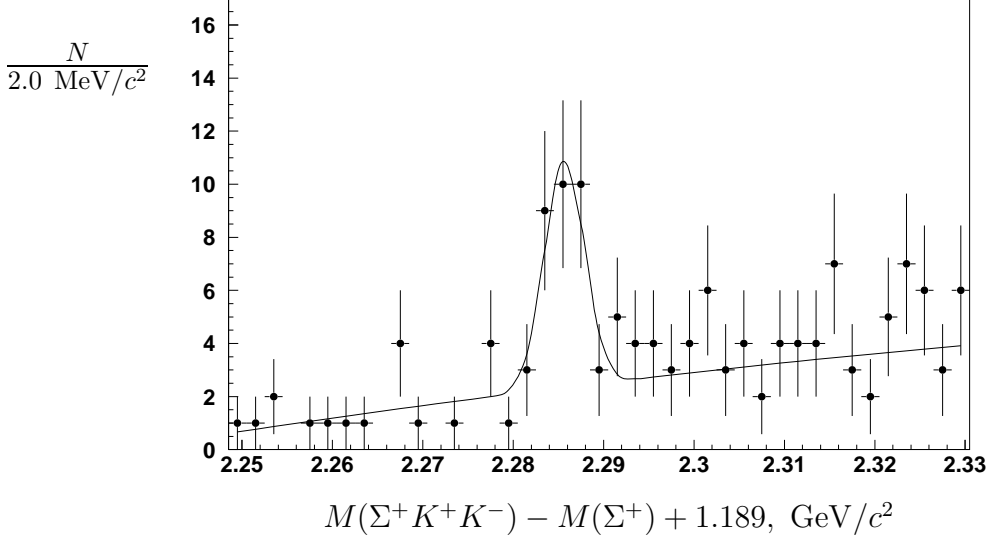


FIG. 10. The $\Sigma^+ K^+ K^-$ invariant mass spectrum, after suppressing $\Sigma^+ \phi$ and $\Xi(1690)^0 K^+$ contributions: the selection requirements and fit are described in the text.

same as for the inclusive $\Sigma^+ K^+ K^-$ mode. Taking into account the systematic error on the K/π identification efficiency, we obtain an upper limit on the branching ratio

$$\mathcal{B}(\Lambda_c^+ \rightarrow \Sigma^+ K^+ K^-)_{non-res} / \mathcal{B}(\Lambda_c^+ \rightarrow \Sigma^+ \pi^+ \pi^-) < 0.017$$

at the 90% confidence level, neglecting possible interference effects between $\Lambda_c^+ \rightarrow \Sigma^+ \phi$ and other resonant decays.

VI. MEASUREMENT OF THE $\Lambda_c^+ \rightarrow p K^+ K^-$ AND $\Lambda_c^+ \rightarrow p \phi$ DECAYS

The first evidence for the $\Lambda_c^+ \rightarrow p \phi$ decay was reported by NA32 in 1990, who claimed a signal of 2.8 ± 1.9 events [6]. The decay $\Lambda_c^+ \rightarrow p K^+ K^-$ was observed for the first time by E687 in 1993, who also obtained an upper limit for the branching ratio of $\Lambda_c^+ \rightarrow p \phi$ [7]. The most recent statistically significant resonant analysis was published by CLEO in 1996, who found the following branching ratios: $\mathcal{B}(\Lambda_c^+ \rightarrow p K^+ K^-) / \mathcal{B}(\Lambda_c^+ \rightarrow p K^- \pi^+) = 0.039 \pm 0.009 \pm 0.007$ and $\mathcal{B}(\Lambda_c^+ \rightarrow p \phi) / \mathcal{B}(\Lambda_c^+ \rightarrow p K^- \pi^+) = 0.024 \pm 0.006 \pm 0.003$ [8].

Reconstructing $\Lambda_c^+ \rightarrow p K^+ K^-$ candidates according to section II, with the kaon cuts tightened to $P(K/\pi) > 0.9$, we see a clear peak at the Λ_c^+ mass, as shown in Fig. 11. The tight $P(K/\pi)$ cut is necessary to suppress the large combinatorial background. We fit the distribution with a gaussian (with width fixed to $2.8 \text{ MeV}/c^2$ from the MC) plus a second order polynomial, and find 446 ± 72 $\Lambda_c^+ \rightarrow p K^+ K^-$ events. For normalization we reconstructed the $\Lambda_c^+ \rightarrow p K^- \pi^+$ decay mode with equivalent cuts (shown in Fig. 12) and fitted the distribution with a double gaussian for the large signal peak, and a second order polynomial, finding 33610 ± 1414 events. The relative efficiency of the $\Lambda_c^+ \rightarrow p K^- K^+$ decay reconstruction with respect to $\Lambda_c^+ \rightarrow p K^+ \pi^-$ was found to be $0.21/0.24 = 0.88$ in the MC: using this value, we extract the branching ratio

$$\mathcal{B}(\Lambda_c^+ \rightarrow p K^+ K^-) / \mathcal{B}(\Lambda_c^+ \rightarrow p K^- \pi^+) = (1.50 \pm 0.25 \pm 0.15) \times 10^{-2}.$$

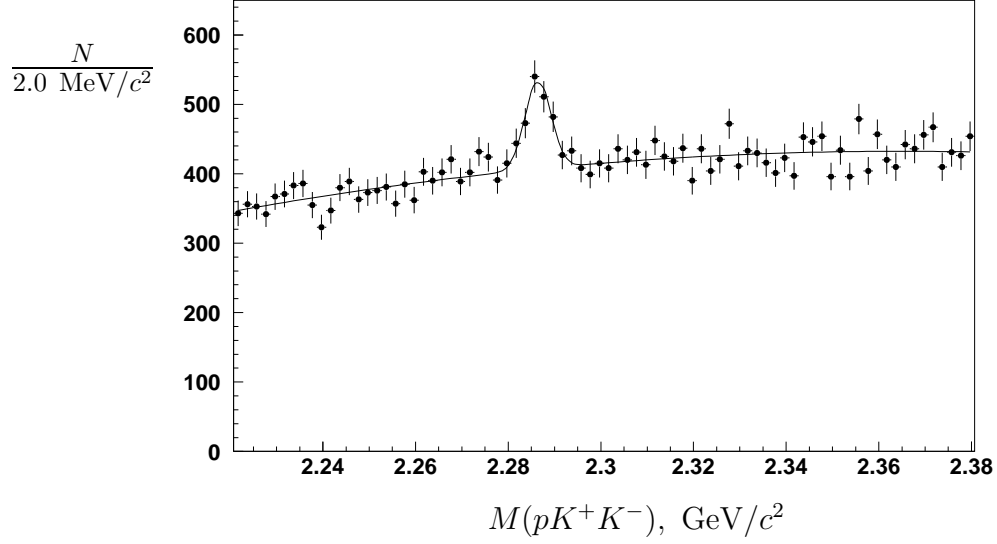


FIG. 11. $\Lambda_c^+ \rightarrow pK^+K^-$: invariant mass spectrum of the selected pK^+K^- combinations.

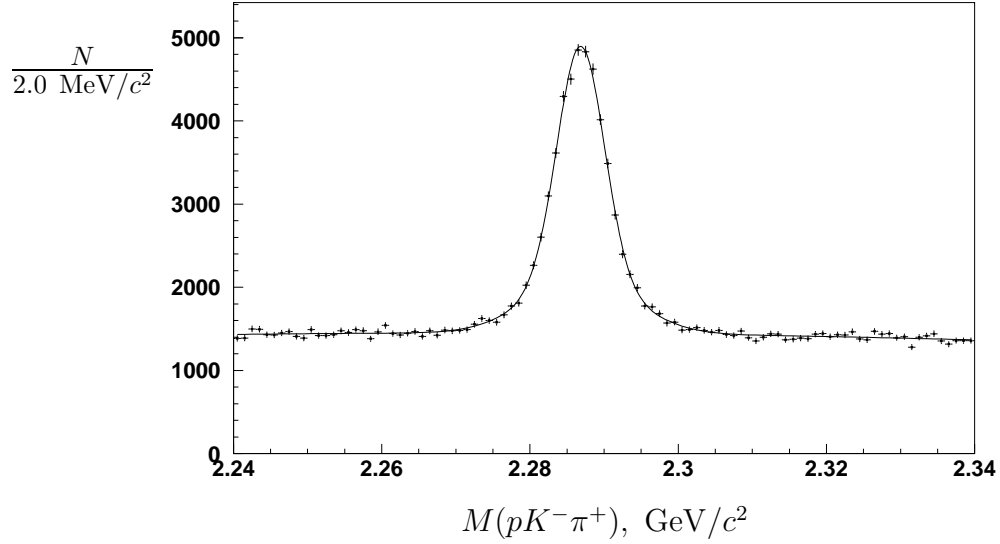


FIG. 12. The invariant mass spectrum for the normalization mode $\Lambda_c^+ \rightarrow pK^-\pi^+$, using equivalent cuts to the $\Lambda_c^+ \rightarrow pK^+K^-$ analysis.

The systematic error is dominated by the uncertainty in the relative K/π identification efficiency.

In order to obtain the $\Lambda_c^+ \rightarrow p\phi$ signal we take pK^+K^- from a $\pm 6 \text{ MeV}/c^2$ ($\pm 2\sigma$) window around the fitted Λ_c^+ mass ($2286 \text{ MeV}/c^2$), and plot the invariant mass of the K^+K^- combination, Fig. 13 (points with error bars); the equivalent distribution is also shown for pK^+K^- from $6 \text{ MeV}/c^2$ sideband intervals $10 \text{ MeV}/c^2$ below and above the fitted Λ_c^+ mass (shaded histogram). The distributions are fitted with a Breit-Wigner function (describing the ϕ signal) convoluted with a gaussian of a fixed width (representing the detector mass resolution) plus a 3rd order polynomial multiplied by a square root threshold factor. The width of the ϕ Breit-Wigner function was fixed to its nominal value [2], and the width of the gaussian was fixed to $1.0 \text{ MeV}/c^2$ based on MC simulation. The fit yields 430 ± 23 events for the ϕ signal in the Λ_c^+ region and 232 ± 17 in the sidebands. To extract the $\Lambda_c^+ \rightarrow p\phi$ contribution we subtract the ϕ yield in the sidebands from the yields in the Λ_c^+ signal region, correcting for the phase space factor obtained from the pK^+K^- background fitting function. After making a further correction for the signal outside the Λ_c^+ mass interval we obtain 205 ± 30 $\Lambda_c^+ \rightarrow p\phi$ decays.

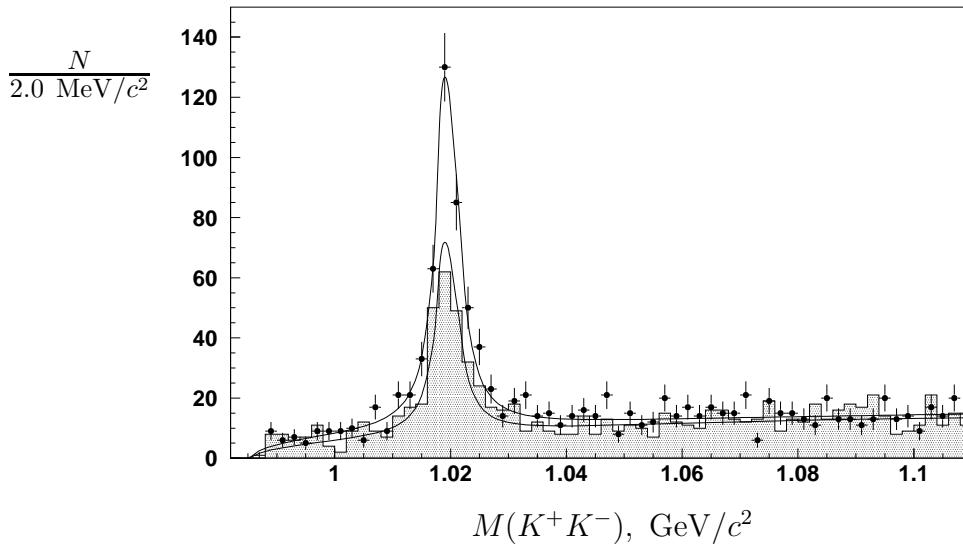


FIG. 13. Fitting for the $\Lambda_c^+ \rightarrow p\phi$ component: the invariant mass spectra of K^+K^- combinations from the $\Lambda_c^+ \rightarrow pK^+K^-$ signal area (points with error bars) and sidebands (shaded histogram). The selection requirements and fit are described in the text.

The reconstruction efficiency of the $\Lambda_c^+ \rightarrow p\phi$ decay relative to $\Lambda_c^+ \rightarrow pK^+\pi^-$ was calculated using the Monte Carlo and found to be $0.20/0.24 = 0.83$. Taking into account the ϕ branching fraction $\mathcal{B}(\phi \rightarrow K^+K^-) = 49.2\%$ [2], we calculate a branching ratio

$$\mathcal{B}(\Lambda_c^+ \rightarrow p\phi)/\mathcal{B}(\Lambda_c^+ \rightarrow pK^-\pi^+) = (1.50 \pm 0.23 \pm 0.15) \times 10^{-2}.$$

The non- ϕ $\Lambda_c^+ \rightarrow pK^+K^-$ signal is estimated by making an invariant mass cut $|M(K^+K^-) - m_\phi| > 10 \text{ MeV}/c^2$ to suppress the $\phi \rightarrow K^+K^-$ contribution: the resulting pK^+K^- mass spectrum is shown in Fig 14. A fit with a gaussian (with width fixed to $2.8 \text{ MeV}/c^2$ from the MC) and a second order polynomial, shown on the figure, yields

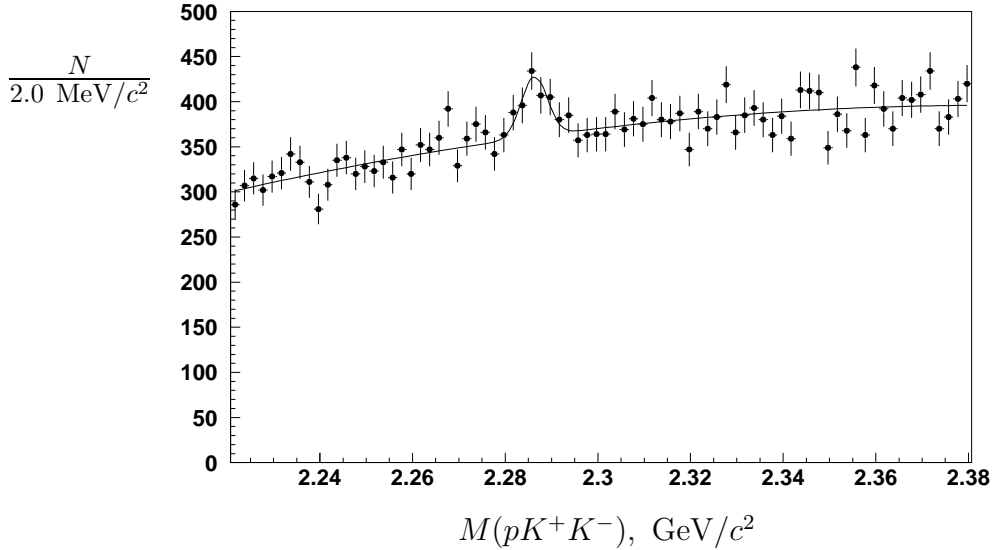


FIG. 14. The $\Lambda_c^+ \rightarrow pK^+K^-$ invariant mass spectrum, after suppressing the $p\phi$ contribution: the selection requirements and fit are described in the text.

234 ± 59 events. Integrating the ϕ Breit-Wigner function over the allowed $M(K^+K^-)$ region, we found that 14% of the total $\Lambda_c^+ \rightarrow p\phi$ signal (27.6 ± 6.2 events) contributes: subtracting these, we have 206 ± 59 events. The phase space correction factor accounting for the missing region around the ϕ mass is found to be 1.075 by MC simulation of the non- ϕ $M(K^+K^-)$ spectrum: applying this correction we obtain 222 ± 64 $\Lambda_c^+ \rightarrow pK^+K^-$ non- ϕ decays. Assuming the relative efficiency for reconstruction of $\Lambda_c^+ \rightarrow pK^+K^-$ (non- ϕ) decays with respect to $\Lambda_c^+ \rightarrow pK^-\pi^+$ to be the same as for inclusive pK^+K^- , we calculate a branching ratio

$$\mathcal{B}(\Lambda_c^+ \rightarrow pK^+K^-)_{\text{non-}\phi} / \mathcal{B}(\Lambda_c^+ \rightarrow pK^-\pi^+) = (0.75 \pm 0.23 \pm 0.08) \times 10^{-2}.$$

As with previous channels, the uncertainty in the relative K/π identification efficiency dominates the systematic error.

VII. CONCLUSIONS

In summary, we report the first observation of the Cabibbo-suppressed decays $\Lambda_c^+ \rightarrow \Lambda^0 K^+$ and $\Lambda_c^+ \rightarrow \Sigma^0 K^+$, and the first observation of $\Lambda_c^+ \rightarrow \Sigma^+ K^+ \pi^-$ with large statistics. The decays $\Lambda_c^+ \rightarrow pK^+K^-$, $\Lambda_c^+ \rightarrow p\phi$ and $\Lambda_c^+ \rightarrow (pK^+K^-)_{\text{non-}\phi}$, and the W-exchange decays $\Lambda_c^+ \rightarrow \Sigma^+ K^+ K^-$ and $\Lambda_c^+ \rightarrow \Sigma^+ \phi^0$ have been measured with the best accuracy to date. We have also observed evidence for the decay $\Lambda_c^+ \rightarrow \Xi(1690)^0 K^+$ and set an upper limit on the non-resonant decay mode $\Lambda_c^+ \rightarrow \Sigma^+ K^+ K^-$. The results for these decay modes are listed in Table 1: all values are preliminary.

TABLE I. Results obtained in this paper.

| Decay mode | Ratio of branching fractions | |
|---|---|---|
| $\Lambda_c^+ \rightarrow \Lambda^0 K^+$ | $\mathcal{B}(\Lambda_c^+ \rightarrow \Lambda^0 K^+)/\mathcal{B}(\Lambda_c^+ \rightarrow \Lambda^0 \pi^+)$ | $= 0.085 \pm 0.012 \pm 0.015$ |
| $\Lambda_c^+ \rightarrow \Sigma^0 K^+$ | $\mathcal{B}(\Lambda_c^+ \rightarrow \Sigma^0 K^+)/\mathcal{B}(\Lambda_c^+ \rightarrow \Sigma^0 \pi^+)$ | $= 0.073 \pm 0.018 \pm 0.016$ |
| $\Lambda_c^+ \rightarrow \Sigma^+ K^+ \pi^-$ | $\mathcal{B}(\Lambda_c^+ \rightarrow \Sigma^+ K^+ \pi^-)/\mathcal{B}(\Lambda_c^+ \rightarrow \Sigma^+ \pi^+ \pi^-)$ | $= 0.059 \pm 0.014 \pm 0.006$ |
| $\Lambda_c^+ \rightarrow \Sigma^+ K^+ K^-$ | $\mathcal{B}(\Lambda_c^+ \rightarrow \Sigma^+ K^+ K^-)/\mathcal{B}(\Lambda_c^+ \rightarrow \Sigma^+ \pi^+ \pi^-)$ | $= 0.075 \pm 0.008 \pm 0.015$ |
| $\Lambda_c^+ \rightarrow \Sigma^+ \phi$ | $\mathcal{B}(\Lambda_c^+ \rightarrow \Sigma^+ \phi)/\mathcal{B}(\Lambda_c^+ \rightarrow \Sigma^+ \pi^+ \pi^-)$ | $= 0.091 \pm 0.014 \pm 0.018$ |
| $\Lambda_c^+ \rightarrow \Xi(1690)^0 K^+$ | $\mathcal{B}(\Lambda_c^+ \rightarrow \Xi(1690)^0 K^+) \times$ $\times \mathcal{B}(\Xi(1690)^0 \rightarrow \Sigma^+ K^-)/\mathcal{B}(\Lambda_c^+ \rightarrow \Sigma^+ \pi^+ \pi^-)$ | $= 0.021 \pm 0.007 \pm 0.004$ |
| $\Lambda_c^+ \rightarrow (\Sigma^+ K^+ K^-)_{\text{non-res}}$ | $\mathcal{B}(\Lambda_c^+ \rightarrow \Sigma^+ K^+ K^-)_{\text{non-res}}/\mathcal{B}(\Lambda_c^+ \rightarrow \Sigma^+ \pi^+ \pi^-)$ | $< 0.017 \text{ @ } 90\% \text{ c.l.}$ |
| $\Lambda_c^+ \rightarrow p K^+ K^-$ | $\mathcal{B}(\Lambda_c^+ \rightarrow p K^+ K^-)/\mathcal{B}(\Lambda_c^+ \rightarrow p K^- \pi^+)$ | $= (1.50 \pm 0.25 \pm 0.15) \times 10^{-2}$ |
| $\Lambda_c^+ \rightarrow p \phi$ | $\mathcal{B}(\Lambda_c^+ \rightarrow p \phi)/\mathcal{B}(\Lambda_c^+ \rightarrow p K^- \pi^+)$ | $= (1.50 \pm 0.23 \pm 0.15) \times 10^{-2}$ |
| $\Lambda_c^+ \rightarrow (p K^+ K^-)_{\text{non-}\phi}$ | $\mathcal{B}(\Lambda_c^+ \rightarrow p K^+ K^-)_{\text{non-}\phi}/\mathcal{B}(\Lambda_c^+ \rightarrow p K^- \pi^+)$ | $= (0.75 \pm 0.23 \pm 0.08) \times 10^{-2}$ |

VIII. ACKNOWLEDGMENT

We wish to thank the KEKB accelerator group for the excellent operation of the KEKB accelerator. We acknowledge support from the Ministry of Education, Culture, Sports, Science, and Technology of Japan and the Japan Society for the Promotion of Science; the Australian Research Council and the Australian Department of Industry, Science and Resources; the Department of Science and Technology of India; the BK21 program of the Ministry of Education of Korea and the CHEP SRC program of the Korea Science and Engineering Foundation; the Polish State Committee for Scientific Research under contract No.2P03B 17017; the Ministry of Science and Technology of Russian Federation; the National Science Council and the Ministry of Education of Taiwan; the Japan-Taiwan Cooperative Program of the Interchange Association; and the U.S. Department of Energy.

REFERENCES

- [1] Y. Kohara, *Nuovo Cim.* **A111**, 67–73, 1998,
M. A. Ivanov *et al.*, *Phys. Rev.* **D57**, 5632–5652, 1998
K.K. Sharma, R.C. Verma, *Phys. Rev.* **D55**, 7067–7074, 1997
T. Uppal *et al.*, *Phys. Rev.* **D49**, 3417–3425, 1994
- [2] D.E. Groom *et al.* (Particle Data Group), *Eur. Phys. J.* **C15**, 1–878, 2000
- [3] K.Abe *et al.* (Belle Collaboration), KEK Progress Report 2000–4 (2000),
to be published in *Nucl. Instr. Meth. A*
- [4] S. Barlag *et al.* (NA32 Collaboration), *Phys. Lett.* **B283**, 465–470, 1992
- [5] P. Avery *et al.* (CLEO Collaboration), *Phys. Rev. Lett.* **71**, 2391–2395, 1993
- [6] S. Barlag *et al.* (NA32 Collaboration), *Z. Phys. C* **48**, 29–45, 1990
- [7] P.L. Frabetti *et al.* (E687 Collaboration), *Phys. Lett.* **B314**, 477–481, 1993
- [8] J. Alexander *et al.* (CLEO Collaboration), *Phys. Rev.* **D53**, 1039–1050, 1996